Coupling between the heavy-fermion superconductor $CeCoIn_5$ and the antiferromagnetic metal $CeIn_3$ through the atomic interface

M. Naritsuka,* S. Nakamura, Y. Kasahara, T. Terashima, R. Peters, and Y. Matsuda
Department of Physics, Kyoto University, Kyoto 606-8502, Japan

(Received 15 April 2019; revised manuscript received 24 June 2019; published 15 July 2019)

To study the mutual interaction between unconventional superconductivity and magnetic order through an interface, we fabricate hybrid Kondo superlattices consisting of alternating layers of the heavy-fermion superconductor $CeCoIn_5$ and the antiferromagnetic (AFM) heavy-fermion metal $CeIn_3$. The strength of the AFM fluctuations is tuned by applying hydrostatic pressure to the $CeCoIn_5(m)/CeIn_3(n)$ superlattices with m and n unit-cell-thick layers of $CeCoIn_5$ and $CeIn_3$, respectively. The superconductivity in $CeCoIn_5$ and the AFM order in $CeIn_3$ coexist in spatially separated layers in the whole thickness and pressure ranges. At ambient pressure, the Néel temperature T_N of the $CeIn_3$ block layers (BLs) of $CeCoIn_5(7)/CeIn_3(n)$ shows little dependence on the thickness n, in sharp contrast to $CeIn_3(n)/LaIn_3(4)$ superlattices, where T_N is strongly suppressed with decreasing n. This suggests that each $CeIn_3$ BL is magnetically coupled by the Ruderman-Kittel-Kasuya-Yosida interaction through the adjacent $CeCoIn_5$ BL and a three-dimensional magnetic state is formed. With applying pressure to $CeCoIn_5(7)/CeIn_3(13)$, T_N of the $CeIn_3$ BLs is suppressed up to 2.4 GPa, showing a similar pressure dependence to that of bulk $CeIn_3$ single crystals. An analysis of the upper critical field reveals that the superconductivity in the $CeCoIn_5$ BLs is barely influenced by the AFM fluctuations in the $CeIn_3$ BLs, even when the $CeIn_3$ BLs are in the vicinity of the AFM quantum critical point. This is in stark contrast to $CeCoIn_5/CeRhIn_5$ superlattices, in which the superconductivity in the $CeCoIn_5$ BLs is profoundly affected by AFM fluctuations in the $CeRhIn_5$ BLs. The present results show that although AFM fluctuations are injected into the $CeCoIn_5$ BLs from the $CeIn_3$ BLs through the interface, they barely affect the force that binds superconducting electron pairs. These results demonstrate that two-dimensional AFM fluctuations are essentially important for the pairing interactions in $CeCoIn_5$.

DOI: 10.1103/PhysRevB.100.024507

I. INTRODUCTION

It is well established that in several compound families, such as high-T_c cuprates, iron pnictides, and heavy-fermion compounds, Cooper pairs are not bound together through phonon exchange but instead through exchange of some other kind, such as spin fluctuations [1–8]. Despite tremendous efforts, however, the interplay between unconventional superconductivity and magnetism still remains largely unexplored in these systems. This includes fascinating electronic phases, where superconductivity and antiferromagnetic (AFM) order, involving the same charge carriers, coexists, and the important question of why superconductivity is often strongest near a quantum critical point (QCP) where the AFM order vanishes in the zero-temperature limit and spin fluctuations become singular [9–13].

By using a recent state-of-the-art molecular beam epitaxy (MBE) technique, we grow artificial Kondo superlattices with alternating layers of heavy-fermion superconductors and conventional metals or heavy-fermion AFM compounds [14,15]. These Kondo superlattices provide a unique opportunity to study the mutual interactions between the unconventional superconducting state and magnetically ordered or conventional metallic states through the atomic interface and thereby seek answers to the above-mentioned questions. Until now, several types of Kondo superlattices containing the heavy-fermion superconductor $CeCoIn_5$ [16] with a layered structure have been fabricated [17–22]. $CeCoIn_5$ has a quasi-two-dimensional (2D) Fermi surface [23], and the presence of quasi-2D AFM fluctuations has been reported in the normal state [24,25]. Furthermore, a superconducting gap with $d_{x^2-y^2}$-wave symmetry has been observed in a variety of experiments [26–31]. The superconducting state is strongly Pauli-limited, as demonstrated by a first-order phase transition at upper critical fields for directions parallel and perpendicular to the *ab* plane [26,32–34]. It is a prototypical system, in which non-Fermi-liquid behaviors in the normal state and unconventional superconductivity are thought to arise from the proximity to an AFM QCP [35–37]. Under pressure, $CeCoIn_5$ moves away from the QCP, and Fermi liquid behavior is recovered.

It has been shown that in superlattices consisting of alternating layers of $CeCoIn_5$ and the conventional metal $YbCoIn_5$ with atomic layer thicknesses [Fig. 1(a)], the Pauli pair-breaking effect is strongly suppressed from that in the bulk of $CeCoIn_5$ single crystals [18,19]. Site-selective nuclear magnetic resonance (NMR) measurements on $CeCoIn_5/YbCoIn_5$ superlattices have reported that AFM fluctuations in the $CeCoIn_5$ block layers (BLs), particularly in the vicinity of the interface, are weakened [38]. These results have been

*naritsuka@scphys.kyoto-u.ac.jp

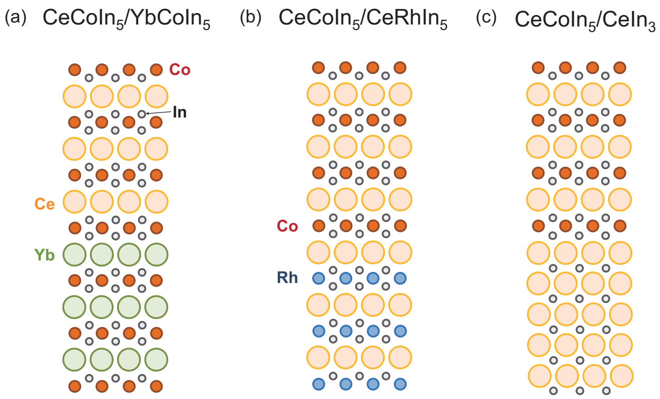

FIG. 1. Schematic representations of three types of Kondo superlattices: (a) $CeCoIn_5/YbCoIn_5$, (b) $CeCoIn_5/CeRhIn_5$, and (c) $CeCoIn_5/CeIn_3$, where $CeCoIn_5$ is a heavy-fermion d-wave superconductor, $YbCoIn_5$ is a conventional metal, and $CeRhIn_5$ and $CeIn_3$ are heavy-fermion AFM metals. The atomic views of the [100] plane are shown.

attributed to the local inversion symmetry breaking at the interface, which results in spin-split Fermi surfaces and thus effectively suppresses the Zeeman effect [18,19,39].

In superlattices consisting of alternating layers of $CeCoIn_5$ and the heavy-fermion AFM metal $CeRhIn_5$ [Fig. 1(b)], the superconducting and AFM states coexist in spatially separated layers. In these superlattices, the influence of local inversion symmetry breaking at the interface has been shown to be less important compared to $CeCoIn_5/YbCoIn_5$. In sharp contrast to $CeCoIn_5/YbCoIn_5$, NMR measurements have revealed that magnetic fluctuations in $CeCoIn_5$ BLs of $CeCoIn_5/CeRhIn_5$ superlattices are enhanced compared to bulk $CeCoIn_5$ single crystal, highlighting the importance of the magnetic proximity effect [40]. In particular, it has been pointed out that in the vicinity of the QCP of $CeRhIn_5$ BLs, AFM fluctuations are enhanced and the force binding superconducting electron-pairs acquires an extremely strong-coupling nature. This indicates that superconducting pairing can be manipulated by magnetic fluctuations injected through the interface [22].

To obtain further insight into the mutual interactions between unconventional superconductivity and magnetic order, we fabricate here superlattices consisting of alternating layers of $CeCoIn_5$ and the AFM metal $CeIn_3$ [Fig. 1(c)]. $CeIn_3$ is an isotropic Kondo lattice material with cubic crystal structure. In bulk $CeIn_3$ single crystals, AFM order with an ordered magnetic moment of $0.48\mu_B$ occurs at $T_N = 10\,\mathrm{K}$, where μ_B is the Bohr magneton [41]. With applying pressure, T_N decreases and vanishes at ~2.6 GPa, indicating an AFM QCP. Superconductivity with a maximum $T_c \approx 200\,\mathrm{mK}$ is induced in a very narrow pressure range around the QCP [9,42].

Our results reveal that, similar to $CeCoIn_5/CeRhIn_5$ but in contrast to $CeCoIn_5/YbCoIn_5$ superlattices, the local inversion symmetry breaking at the interface has only a little effect on the superconductivity in $CeCoIn_5/CeIn_3$ superlattices. However, we find that the magnetic and the superconducting properties in $CeCoIn_5/CeIn_3$ are in marked contrast to those in $CeCoIn_5/CeRhIn_5$ superlattices [22]. Although the AFM fluctuations are injected into the $CeCoIn_5$ BLs from the $CeIn_3$ BLs through the interfaces, they barely affect the electron pairing interactions in the $CeCoIn_5$ BLs. These results provide compelling evidence that 2D AFM fluctuations are essentially important for the superconductivity in $CeCoIn_5$.

II. EXPERIMENTAL DETAILS

The hybrid superlattices $CeCoIn_5(7)/CeIn_3(n)$ ($n = 3$, 4, 6 and 13) with c axis oriented structure are grown on a MgF_2 substrate by the MBE technique [14,15]. We first grow ~20 unit-cell-thick (UCT) $CeIn_3$ (~10 nm) as a buffer layer on MgF_2. Then 7-UCT $CeCoIn_5$ and n-UCT $CeIn_3$ ($n = 3$, 4, 6 and 13) are grown alternatively with total thicknesses of approximately 200 nm. As the epitaxial growth temperature of $CeCoIn_5$ and $CeIn_3$ layers are different, $CeCoIn_5$ and $CeIn_3$ BLs were grown at 570 and 420 °C, respectively. The superlattice is capped with ~5 nm Co to prevent oxidation. A streak pattern of the reflection high-energy electron diffraction (RHEED) image shown in Fig. 2(a) was observed throughout the growth of the superlattices, indicating good epitaxy. The atomic force microscope measurements reveal that the surface roughness is within ±1 nm, which is comparable to 1–2 UCT along the c axis of the constituents. Because atomically flat regions extend over distances of ~0.1 μm, it can be expected that transport properties are not seriously influenced by the roughness. Figure 2(b) displays a high-resolution cross-sectional transmission electron microscope (TEM) image along the (100) direction for the $CeCoIn_5(7)/CeIn_3(13)$ superlattice. A clear interface between the $CeCoIn_5$ and the $CeIn_3$ layers is observed. Figure 2(c) displays an electron energy loss spectroscopy (EELS) image of the same superlattice. The EELS images clearly resolve the 7-UCT $CeCoIn_5$ and the 13-UCT $CeIn_3$ BLs, demonstrating sharp interfaces with no atomic interdiffusion between the neighboring $CeCoIn_5$ and $CeIn_3$ BLs. Figure 2(d) shows the x-ray diffraction patterns for $CeCoIn_5(7)/CeIn_3(n)$ superlattices. The shoulder structure shown by the red arrows near the [003] peak of $CeCoIn_5$ (blue arrows) is consistent with the superlattice structure. These results demonstrate the successful fabrication of epitaxial superlattices with sharp interfaces. High-pressure resistivity measurements have been performed under pressure up to 2.4 GPa using a piston cylinder cell with Daphne oil 7373 as the pressure-transmitting medium. The pressure has been measured by the T_c of Pb.

III. RESULTS

Figure 3(a) depicts the temperature dependence of the resistivity ρ of $CeCoIn_5(7)/CeIn(n)$ superlattices with $n = 3$, 4, 6 and 13. We also show ρ of $CeCoIn_5$ and $CeIn_3$ thin films grown by MBE. The mean free path of these superlattices is difficult to estimate because of the parallel conductions of $CeCoIn_5$ and $CeIn_3$ BLs. However, the mean free path in each BL is expected to be shorter than the atomically flat regions extending over distances of ~0.1 μm, because of the following reasons. In $CeCoIn_5$ and $CeIn_3$ single crystals, the mean free path determined by the de Haas–van Alphen oscillations is ~0.2 μm [43,44]. The residual resistivity ratio of $CeCoIn_5$ and $CeIn_3$ thin films with 100 nm thickness is four to five times smaller than that of the single crystals. Therefore, the mean free path of $CeCoIn_5$ and $CeIn_3$ BLs in the

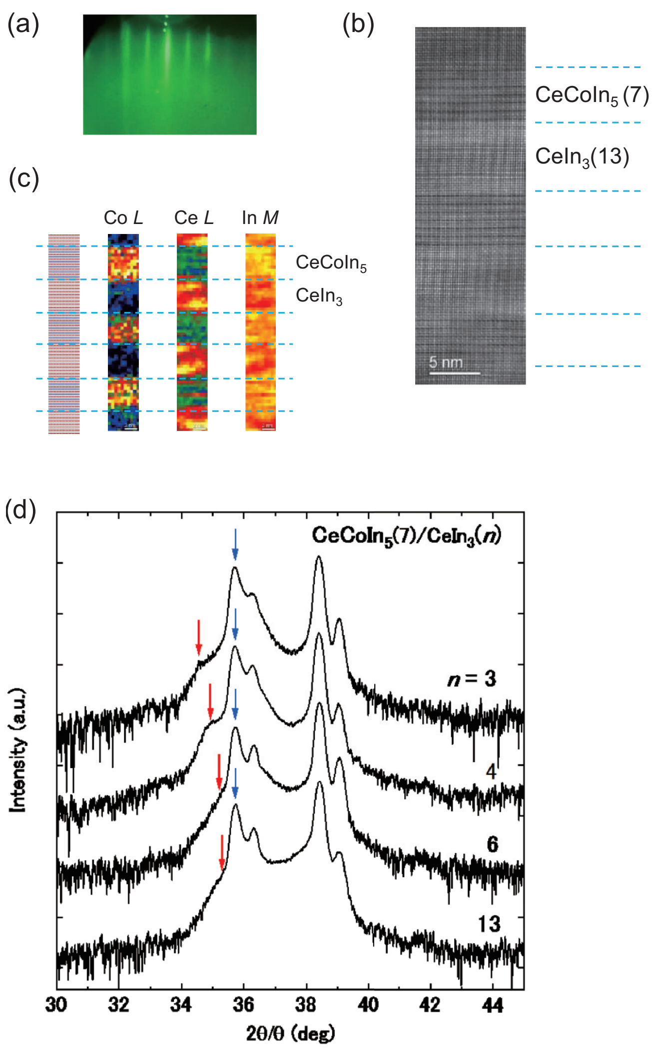

FIG. 2. (a) Typical RHEED streak patterns for $CeCoIn_5(7)/CoIn_3(13)$ superlattice taken during the crystal growth. (b), (c) High-resolution cross-sectional (b) TEM image and (c) EELS images for the $CeCoIn_5(7)/CoIn_3(13)$ superlattice with the electron beam aligned along the (100) direction. The EELS images were taken for Co L, Ce L, and In M edges. (d) Cu $K\alpha_1$ x-ray diffraction patterns for $CeCoIn_5(7)/CoIn_3(n)$ superlattices ($n = 3$, 4, 6, and 13). The blue and red arrows indicate the [003] peaks of $CeCoIn_5$ and satellite peaks due to the superlattice structure, respectively.

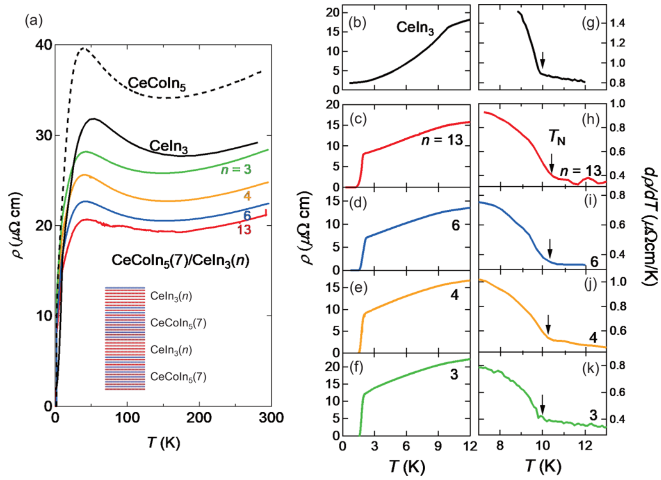

FIG. 3. (a) Temperature dependence of the resistivity $\rho(T)$ in $CeCoIn_5(7)/CeIn_3(n)$ superlattices for $n = 3$, 4, 6, and 13, along with $\rho(T)$ for $CeIn_3$ (black solid line) and $CeCoIn_5$ (black dashed line) thin films. The inset illustrates the schematics of $CeCoIn_5(7)/CeIn_3(n)$ superlattice. (b)–(f) $\rho(T)$ at low temperatures. (g)–(k) Temperature derivative of the resistivity, $d\rho(T)/dT$, as a function of temperature. The arrows indicate the Néel temperature T_N.

superlattices is expected to be much shorter than 0.1 μm, suggesting that the transport properties are not seriously influenced by the surface roughness. The resistivity of $CeCoIn_5(7)/CeIn(n)$ superlattices follows the typical heavy-fermion behavior. With decreasing temperature, $\rho(T)$ increases below $\sim$150 K due to the Kondo scattering but then begins to decrease due to strong c-f hybridization between f-electrons and conduction (c) band electrons, leading to the narrow f-electron band at the Fermi level. The Kondo coherence temperature T_{coh}, at which the heavy-fermion formation occurs, is estimated from the maximum in $\rho(T)$. As shown in Fig. 3(a), T_{coh} of $CeCoIn_5(7)/CeIn(n)$ superlattices is nearly independent of n and is closer to T_{coh} of $CeCoIn_5$ thin film than T_{coh} of $CeIn_3$ thin film, suggesting that T_{coh} is mainly determined by $CeCoIn_5$ BLs. Figures 3(b)–3(f) depict $\rho(T)$ at low temperatures. All superlattices show the superconducting transition at $T \approx 1.5$ K. For the $n = 3$ and 4 superlattices, $\rho(T)$ decreases with increasing slope, $d\rho(T)/dT$, as the temperature is lowered below 12 K down to T_c.

Despite a larger lattice mismatch along the a axis between $CeCoIn_5$ ($a = 0.461$ nm) and $CeIn_3$ ($a = 0.469$ nm) compared to that between $CeCoIn_5$ and $CeRhIn_5$ ($a = 0.466$ nm), T_c of $CeCoIn_5/CeIn_3$ superlattices is close to the T_c of $CeCoIn_5/CeRhIn_5$ superlattices. This implies that the strain effect at the interfaces is not important for T_c. Figures 3(g)–3(k) display the temperature derivative of the resistivity $d\rho(T)/dT$. As shown by the arrows in Fig. 3(g), $d\rho(T)/dT$ of $CeIn_3$ thin film exhibits a distinct kink at $T_N = 10$ K [41]. Similar kink structures are observed in all superlattices at the temperatures indicated by arrows, showing the AFM transition.

Figure 4 shows the thickness dependence of T_N of the $CeCoIn_5(7)/CeIn_3(n)$ superlattices. For comparison, the data sets of $CeIn_3(4)/LaIn_3(n)$, where $LaIn_3$ is a nonmagnetic conventional metal with no f-electrons [14], and $CeCoIn_5(n)/CeRhIn_5(n)$ are also included in the figure. Remarkably, the observed thickness dependence of T_N in $CeCoIn_5/CeIn_3$ is in striking contrast to that in $CeIn_3/LaIn_3$; while T_N is strongly suppressed with decreasing n and vanishes at $n = 2$ in $CeIn_3/LaIn_3$, T_N is nearly independent of n in $CeCoIn_5(7)/CeIn_3(n)$. This suggests that $CeIn_3$ BLs are coupled weakly by the Ruderman-Kittel-Kasuya-Yosida (RKKY) interactions through the adjacent $LaIn_3$ BL, but they can strongly couple through the adjacent $CeCoIn_5$ BL. This is even more surprising, as the distance between different $CeIn_3$ BLs is larger in the $CeCoIn_5(7)/CeIn_3(n)$ superlattices than in the $CeIn_3(n)/LaIn_3(4)$ superlattices. We thus conclude that small but finite magnetic moments are induced

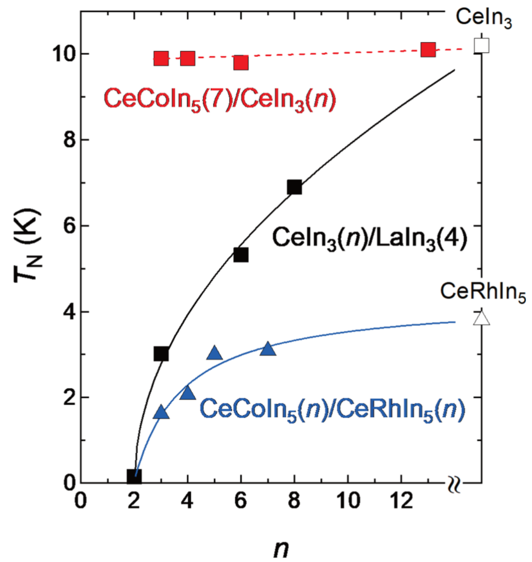

FIG. 4. The Néel temperature T_N for CeCoIn$_5$(7)/CeIn$_3$(n) as a function of n. For comparison, T_N for CeIn$_3$(n)/LaIn$_3$(4) and CeCoIn$_5$(n)/CeRhIn$_5$(n) are shown. Open square and triangle are T_N of bulk CeIn$_3$ and CeRhIn$_5$ single crystals, respectively.

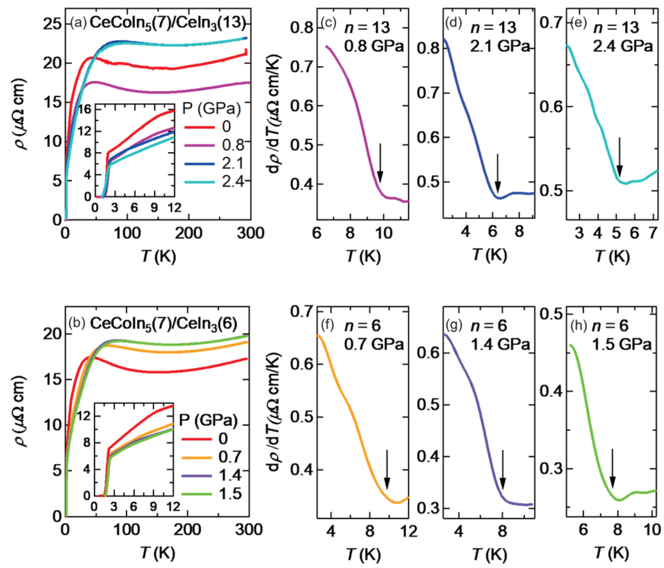

FIG. 5. (a), (e) Temperature dependence of the resistivity $\rho(T)$ under pressure for CeCoIn$_5$(7)/CeIn$_3$(n) for (a) $n = 13$ and (e) $n = 6$. Inset: $\rho(T)$ at low temperatures. (b)–(d) and (f)–(h) show the temperature derivative of the resistivity, $d\rho(T)/dT$, as a function of temperature under pressure for $n = 13$ and 6, respectively. The arrows indicate the Néel temperature T_N.

in CeCoIn$_5$ BLs in CeCoIn$_5$/CeIn$_3$, which mediate the RKKY interaction. On the other hand, because of the absence of strongly interacting f-electrons in LaIn$_3$, which can form magnetic moments, the RKKY interaction in CeIn$_3$/LaIn$_3$ can be expected to be much weaker. To clarify this, a microscopic probe of magnetism, such as NMR measurements, is required. We note that as shown in Fig. 4, the reduction of T_N is also observed in CeCoIn$_5$(n)/CeRhIn$_5$(n) superlattices [22], suggesting that the RKKY interaction between CeRhIn$_5$ BLs through adjacent CeCoIn$_5$ BL is negligibly small. This is supported by the recent site-selective NMR measurements, which report no discernible magnetic moments induced in the CeCoIn$_5$ BLs in CeCoIn$_5$/CeRhIn$_5$ [40].

The pressure dependence of the superconducting and magnetic properties provide crucial information on the mutual interaction between superconductivity and magnetism through the interface. Figures 5(a) and 5(b) and their insets show the temperature dependence of $\rho(T)$ under pressure for CeCoIn$_5$(7)/CeIn$_3$(n) for $n = 13$ and 6, respectively. With the application of pressure, the temperature at which $\rho(T)$ shows its maximum increases due to the enhancement of the c-f hybridization [36]. As shown in the insets, both superlattices undergo a superconducting transition under pressure. Figures 5(c)–5(e) and 5(f)–5(h) show $d\rho(T)/dT$ under pressure for $n = 13$ and 6, respectively. Clear kink structure associated with the AFM transition can be seen in the data.

Figure 6(a) depicts the pressure dependence of T_N and T_c for CeCoIn$_5$(7)/CeIn$_3$(n) superlattices for $n = 6$ and 13. With applying pressure, T_N decreases rapidly. For comparison, T_N of a bulk single crystal CeIn$_3$ is also shown by the solid line [9]. The pressure dependence of T_N of both superlattices is very similar to that of the bulk CeIn$_3$ single crystal. In bulk CeIn$_3$ crystal, the AFM QCP is located at $p_c \approx 2.6$ GPa. It is natural to expect, therefore, that the AFM QCP of the superlattices is close to 2.6 GPa. Thus, at 2.4 GPa, the superlattices are in the vicinity of the AFM QCP. This is supported by the temperature dependence of the resistivity under pressure. The resistivity can be fitted as

$$\rho(T) = \rho_0 + AT^{\varepsilon}. \quad (1)$$

Figure 6(b) shows the pressure dependence of ε obtained from $d \ln \Delta\rho / d \ln T$, where $\Delta\rho = \rho(T) - \rho_0$. The magnitude of ε decreases with pressure. In bulk CeIn$_3$ single crystal, ε decreases with pressure and exhibits a minimum at the AFM QCP [9,42]. On the other hand, applying pressure to CeCoIn$_5$

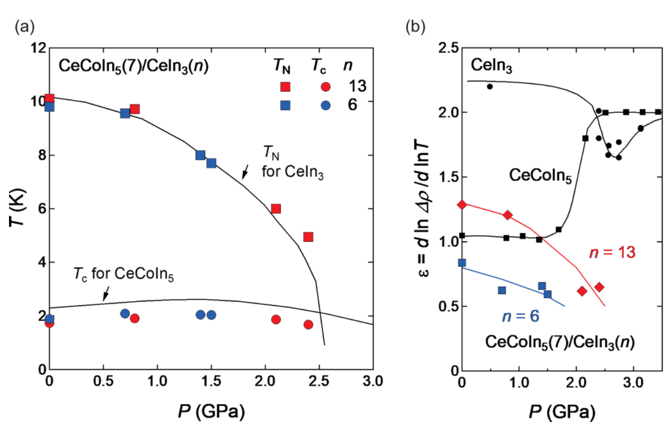

FIG. 6. (a) Pressure dependence of T_N and T_c of CeCoIn$_5$(7)/CeIn$_3$(n) superlattices for $n = 13$ and 6. For comparison, T_N of CeIn$_3$ and T_c of CeCoIn$_5$ single crystals are shown by solid lines. (b) Pressure dependence of the exponent ε in $\rho(T) = \rho_0 + AT^{\varepsilon}$, obtained from $d \ln \Delta\rho / d \ln T$ ($\Delta\rho = \rho(T) - \rho_0$), for the CeCoIn$_5$(7)/CeIn$_3$($n$) superlattices for $n = 13$ and 6. For comparison, ε for bulk CeIn$_3$ and CeCoIn$_5$ single crystals is shown.

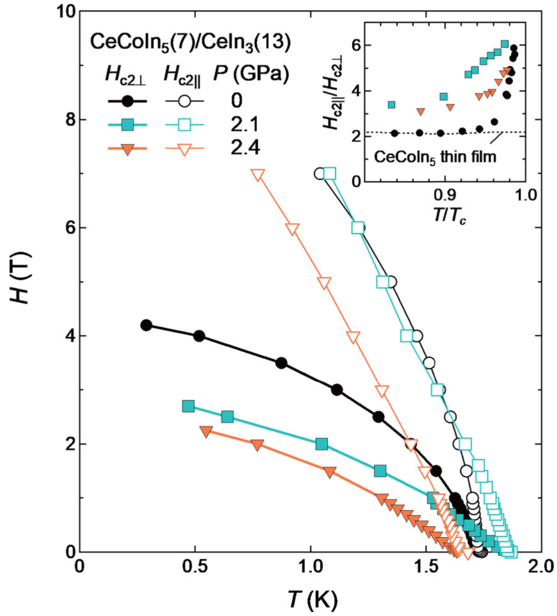

FIG. 7. Temperature dependence of upper critical fields in magnetic fields parallel ($H_{c2\parallel}$, open symbols) and perpendicular ($H_{c2\perp}$, closed symbols) to the *ab*-plane for $CeCoIn_5(7)/CeIn_3(13)$ superlattice at ambient pressure and at 2.1 and 2.4 GPa. The inset shows anisotropy of the upper critical field, $H_{c2\parallel}/H_{c2\perp}$. The data of $CeCoIn_5$ thin film at ambient pressure are shown by dotted line.

leads to an increase of ε, which is attributed to the suppression of the non-Fermi-liquid behavior, $\rho(T) \propto T$, and the development of a Fermi liquid state with its characteristic $\rho(T) \propto T^2$ dependence [35,36].

Therefore, the reduction of ε with pressure arises from the $CeIn_3$ BLs, indicating that the $CeIn_3$ BLs approach the AFM QCP.

As shown in Fig. 6(a), T_c increases, peaks at ~1.8 GPa, and then decreases when applying pressure. This pressure dependence bears a resemblance to that of $CeCoIn_5$ bulk single crystals [35]. An analysis of the upper critical field provides important information about the superconductivity of $CeCoIn_5$ BLs. Figure 7 depicts the temperature dependence of the upper critical field determined by the midpoint of the resistive transition in a magnetic field $\boldsymbol{H}$ applied parallel ($H_{c2\parallel}$) and perpendicular ($H_{c2\perp}$) to the layers. The inset of Fig. 7 shows the anisotropy of the upper critical fields $H_{c2\parallel}/H_{c2\perp}$ at ambient pressure. The anisotropy diverges on approaching T_c. This is in sharp contrast to the $CeCoIn_5$ thin film, whose anisotropy is nearly temperature-independent up to T_c. The observed diverging anisotropy indicates that the superconducting electrons are confined in the 2D $CeCoIn_5$ BLs. In fact, in 2D superconductivity, $H_{c2\parallel}$ is limited by Pauli paramagnetic pair breaking and increases as $\sqrt{T_c - T}$, while $H_{c2\perp}$ increases as $T_c - T$ due to the orbital pair breaking near T_c [17]. Moreover, the thickness of the $CeCoIn_5$ BL is comparable to the coherence length perpendicular to the layer, $\xi_c \sim 4$ nm. Thus each 7-UCT $CeCoIn_5$ BL effectively behaves as a 2D superconductor.

IV. DISCUSSION

It has been revealed that the temperature dependence of $H_{c2\perp}$ provides crucial information about the impact of the interface on the superconductivity in $CeCoIn_5$ BLs. In particular, the modification of the Pauli paramagnetic effect in the superlattice, which dominates the pair breaking in bulk $CeCoIn_5$ single crystals, gives valuable clues [18,19,21,22]. Figures 8(a) and 8(b) depict the T dependence of the $H_{c2\perp}$ of $CeCoIn_5(7)/CeIn_3(13)$ superlattice, normalized by the orbital-limited upper critical field at zero temperature, $H_{c2\perp}^{orb}(0)$, which is obtained from the Werthamer-Helfand-Hohenberg (WHH) formula, $H_{c2\perp}^{orb}(0) = -0.69T_c(dH_{c2\perp}/dT)_{T_c}$ [45]. In Figs. 8(a) and 8(b), two extreme cases are also included: the WHH curve with no Pauli pair-breaking and $H_{c2}/H_{c2\perp}^{orb}(0)$ for bulk $CeCoIn_5$ single crystal [32]. For comparison, $H_{c2\perp}^{orb}(0)$ for $CeCoIn_5/YbCoIn_5$ and $CeCoIn_5/CeRhIn_5$ are also shown [17,22].

At ambient pressure, $H_{c2\perp}/H_{c2\perp}^{orb}(0)$ of $CeCoIn_5/YbCoIn_5$ and $CeCoIn_5/CeRhIn_5$ are strongly enhanced from that of $CeCoIn_5$ bulk single crystals, indicating the suppression of the Pauli paramagnetic pair-breaking effect. However, it has been pointed out that the mechanisms of this suppression in these two systems are essentially different. In $CeCoIn_5/YbCoIn_5$, the enhancement of $H_{c2\perp}/H_{c2\perp}^{orb}(0)$ is caused by the local inversion symmetry breaking at the interface [18,39]. The asymmetry of the potential perpendicular to the 2D plane of the superlattice, $\nabla V \parallel [001]$, induces the Rashba spin-orbit interaction $\alpha_R = \boldsymbol{g}(\boldsymbol{k}) \cdot \boldsymbol{\sigma} \propto (\boldsymbol{k} \times \nabla V) \cdot \boldsymbol{\sigma}$, where $\boldsymbol{g}(\boldsymbol{k}) = (k_y, -k_x, 0)/k_F$, where k_F and $\boldsymbol{\sigma}$ are the Fermi wave number and the Pauli matrices, respectively. The Rashba spin-orbit interaction splits the Fermi surface into two sheets with different spin textures [46]. The energy splitting is given by α_R, and the spin direction is tilted into the 2D plane, rotating clockwise on one sheet and anticlockwise on the other. When the Rashba splitting exceeds the superconducting gap energy ($\alpha_R > \Delta$), the superconducting state is dramatically modified [39,46,47]. In particular, when the magnetic field is applied perpendicular to the 2D plane, the magnetic field does not couple to the spins, leading to a suppression of the Pauli pair-breaking effect. At $p = 2.2$ GPa, $H_{c2\perp}/H_{c2\perp}^{orb}(0)$ of $CeCoIn_5/YbCoIn_5$ nearly coincides with the WHH curve. This indicates that $H_{c2\perp}$ is dominated by the orbital pair breaking most likely due to the suppression of the Pauli paramagnetic pair-breaking effect by the Rashba splitting.

On the other hand, in $CeCoIn_5/CeRhIn_5$ superlattices, it has been shown that the effect of the local inversion symmetry breaking on $H_{c2\perp}$ is less important compared with $CeCoIn_5/YbCoIn_5$ [22]. It has been proposed that magnetic fluctuations (paramagnons) in $CeRhIn_5$ BLs injected through the interface dramatically enhance the force binding superconducting electron pairs in $CeCoIn_5$ BLs, leading to the enhancement of Δ. As a result, the Pauli limiting field $H_{c2\perp}^{Pauli}$ $(=\sqrt{2}\Delta/g\mu_B)$ is enhanced, where g is the g-factor of the electrons. This increases the relative importance of the orbital pair-breaking effect, giving rise to the enhancement of $H_{c2\perp}/H_{c2\perp}^{orb}(0)$ [22]. At $p = 2.1$ GPa, which is close to the AFM QCP of $CeRhIn_5$ BLs, $H_{c2\perp}/H_{c2\perp}^{orb}(0)$ nearly coincides with the WHH curve. This has been attributed to the enhanced

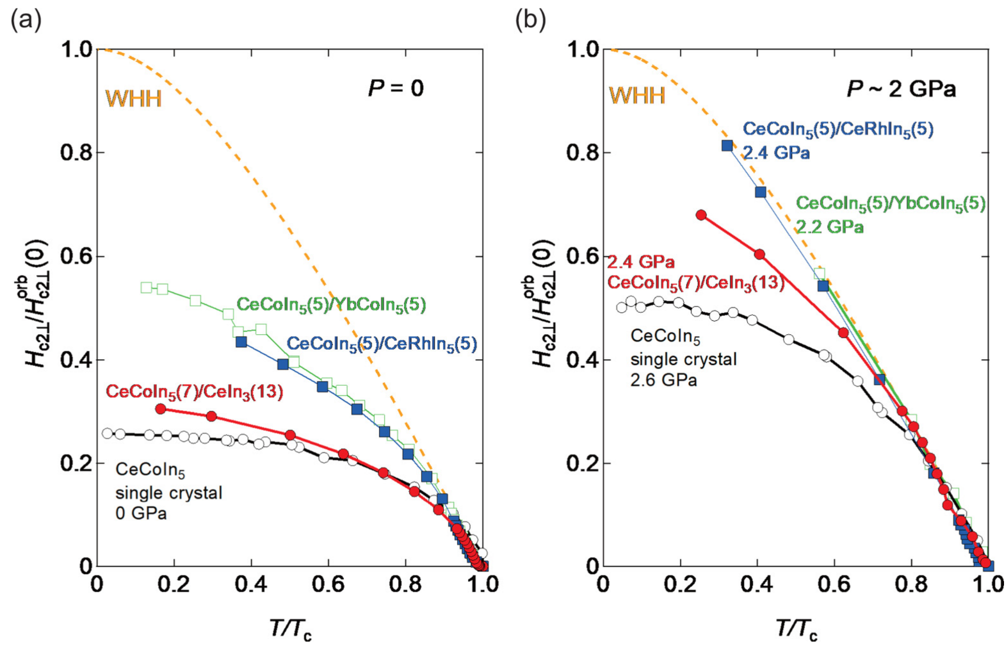

FIG. 8. (a) Upper critical field in perpendicular field normalized by the orbital limiting upper critical field, $H_{c2\perp}/H_{c2\perp}^{\rm orb}(0)$, plotted as a function of T/T_c (a) at ambient pressure and (b) under pressure about 2 GPa for $CeCoIn_5(7)/CeIn_3(13)$ superlattices. For comparison, $H_{c2\perp}/H_{c2\perp}^{\rm orb}(0)$ for bulk $CeCoIn_5$ single crystal, $CeCoIn_5(5)/YbCoIn_5(5)$, and $CeCoIn_5(5)/CeRhIn_5(5)$ are shown. Orange dotted lines represent the WHH curve, which is the upper critical field for purely orbital limiting.

Pauli limiting field that well exceeds the orbital limiting field ($H_{c2\perp}^{\rm Pauli} \gg H_{c2\perp}^{\rm orb}$) [22].

In contrast to $CeCoIn_5/YbCoIn_5$ and $CeCoIn_5/CeRhIn_5$, $H_{c2\perp}/H_{c2\perp}^{\rm orb}(0)$ is only slightly enhanced in $CeCoIn_5(7)/CeIn_3(13)$ superlattice at ambient pressure from that of bulk $CeCoIn_5$ single crystal. This indicates that $H_{c2\perp}$ is dominated by the Pauli paramagnetic effect, i.e., $H_{c2\perp} \approx H_{c2\perp}^{\rm Pauli} \ll H_{c2\perp}^{\rm orb}$. This implies that the effect of local inversion symmetry breaking on the superconductivity in $CeCoIn_5/CeIn_3$ is weak compared with $CeCoIn_5/YbCoIn_5$. The local inversion symmetry is broken for the $CeCoIn_5/YbCoIn_5$ on the CoIn-layer while it is broken on the Ce layer for $CeCoIn_5/CeIn_3$ and $CeCoIn_5/CeRhIn_5$. Therefore, the present results suggest that the inversion symmetry breaking on the CoIn layer induces a larger local electric field gradient. Moreover, superconducting electrons in $CeCoIn_5$ BLs are not strongly influenced by the AFM order in $CeIn_3$ BLs compared with $CeCoIn_5/CeRhIn_5$.

When superconductivity is dominated by the Pauli-limiting effect ($H_{c2\perp} \approx H_{c2\perp}^{\rm Pauli}$), $2\Delta/k_BT_c$ is estimated as

$$\frac{2\Delta}{k_BT_c} \approx \sqrt{2}\frac{g\mu_B H_{c2\perp}}{k_BT_c}. \tag{2}$$

Figure 9 depicts the pressure dependence of $q = \sqrt{2}g\mu_B H_{c2\perp}/k_BT_c$ for $CeCoIn_5/CeRhIn_5$ and $CeCoIn_5/CeIn_3$, along with q for bulk $CeCoIn_5$ single crystal. Here $g = 2$ is assumed. Although this simple assumption should be scrutinized, the fact that $q = 4.2$ of the bulk $CeCoIn_5$ is larger than the BCS value of $q = 3.54$ is consistent with the strong-coupling superconductivity, which is supported by the specific-heat measurements that report $2\Delta/k_BT_c \approx 6$ [16]. The increase of q with pressure in $CeCoIn_5/CeRhIn_5$ implies the increase of $2\Delta/k_BT_c$. This increase has been attributed to an enhancement of the force binding superconducting electron pairs. In spin fluctuation mediated superconductors, the pairing interaction is mainly provided by high-energy fluctuations, while low-energy fluctuations act as pair breaking. In this case, an increase of $2\Delta/k_BT_c$ occurs without

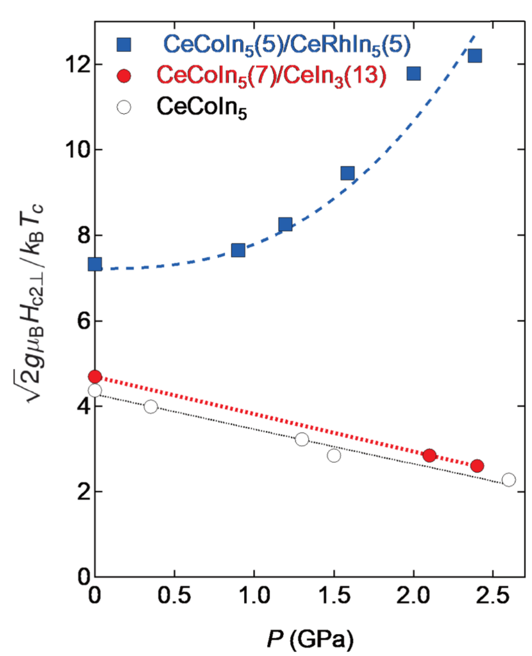

FIG. 9. Pressure dependence of $q = \sqrt{2}g\mu_B H_{c2\perp}/k_BT_c \approx 2\Delta/k_BT_c$ for $CeCoIn_5(7)/CeIn_3(13)$ superlattice. For comparison, q of bulk $CeCoIn_5$ single crystal and $CeCoIn_5(5)/CeRhIn_5(5)$ are plotted.

accompanying a large enhancement of T_c, which is consistent with the results of $CeCoIn_5/CeRhIn_5$ [22]. Thus, the critical AFM fluctuations that develop in $CeRhIn_5$ BLs near the QCP are injected into the $CeCoIn_5$ BLs through the interface and strongly enhance the pairing interaction in $CeCoIn_5$ BLs.

In stark contrast to $CeCoIn_5/CeRhIn_5$ superlattices, q decreases with pressure in bulk $CeCoIn_5$ single crystal. This implies that the pairing interaction is weakened with applying pressure, which is consistent with the fact that the pressure moves the system away from the QCP of $CeCoIn_5$. The reduction of $2\Delta/k_BT_c$ with pressure in bulk $CeCoIn_5$ single crystals is confirmed by the jump of the specific heat at T_c [48]. It should be stressed that the pressure dependence of q in $CeCoIn_5(7)/CeIn_3(13)$ is very similar to that of bulk $CeCoIn_5$. This strongly indicates that the pairing interactions in $CeCoIn_5$ BLs are barely influenced by AFM fluctuations injected from the adjacent $CeIn_3$ BLs through the interface even when $CeIn_3$ BLs are located near the AFM QCP.

The most salient feature in the $CeCoIn_5/CeIn_3$ superlattices is that the superconductivity of $CeCoIn_5$ BLs is little affected by the critical AFM fluctuations in $CeIn_3$ BLs, despite the fact that AFM fluctuations are injected from the adjacent $CeIn_3$ BLs into $CeCoIn_5$ BLs, as evidenced by the AFM order in $CeCoIn_5/CeIn_3$ demonstrating that different $CeIn_3$ BLs are magnetically coupled by the RKKY interaction through adjacent $CeCoIn_5$ BLs. Even in the vicinity of the AFM QCP of the $CeIn_3$ BLs, the superconducting state in the $CeCoIn_5$ BLs is very similar to that of $CeCoIn_5$ bulk single crystals. This indicates that the AFM fluctuations injected from $CeIn_3$ BLs do not help to enhance the force binding the superconducting electron pairs in $CeCoIn_5$ BLs. This is in stark contrast to $CeCoIn_5/CeRhIn_5$, in which the pairing force in $CeCoIn_5$ BL is strongly enhanced by the AFM fluctuations in $CeRhIn_5$ BLs [22], although the $CeRhIn_5$ BLs are magnetically only weakly coupled through $CeCoIn_5$ BLs.

The contrasting behaviors between $CeCoIn_5/CeIn_3$ and $CeCoIn_5/CeRhIn_5$ superlattices suggest that there are two possible important factors that determine whether magnetic fluctuations are injected through the interface: one is the magnetic wave vector and the other is the matching of the Fermi surface between two materials. For $CeCoIn_5$, the Fermi surface is 2D-like, and AFM fluctuations with wave vector $\boldsymbol{q}_0 = (0.45, 0.45, 0.5)$ are dominant [25]. The magnetic wave vector in the ordered phase of $CeIn_3$ is commensurate with $\boldsymbol{q}_0 = (0.5, 0.5, 0.5)$ [41]. The evolution of the ordered moment below T_N is consistent with mean-field theory. While the wave number along the c axis, q_c, of $CeIn_3$ is the same as that of $CeCoIn_5$, the 3D Fermi surface of $CeIn_3$ is very different from the 2D Fermi surface of $CeCoIn_5$. On the other hand, for $CeRhIn_5$, $\boldsymbol{q}_0$ in the ordered phase is incommensurate, $\boldsymbol{q}_0 = (0.5, 0.5, 0.297)$, at low pressure [49] and changes to $\boldsymbol{q}_0 = (0.5, 0.5, 0.4)$ above $\sim$1.0 GPa [50]. Thus, the q_c of $CeRhIn_5$ is different from the q_c of $CeCoIn_5$. The evolution of the ordered moment below T_N deviates from mean-field behavior, likely due to 2D fluctuations. However, the 2D Fermi surface of $CeRhIn_5$ bears a close resemblance to that of $CeCoIn_5$.

The equality between the c axis component of $\boldsymbol{q}_0$ in $CeCoIn_5$ and $CeIn_3$ would explain why the magnetic coupling between $CeIn_3$ BLs through a $CeCoIn_5$ BL is stronger than that between $CeRhIn_5$ BLs. Thus, AFM order is formed in $CeCoIn_5(7)/CeIn_3(n)$ even for small n, for which the AFM order has already vanished in $CeCoIn_5(n)/CeRhIn_5(n)$. In magnetically mediated superconductors, the pairing interaction is expected to be strongly wave-number-dependent. Considering the good resemblance of the Fermi surface and the same $d_{x^2-y^2}$ superconducting gap symmetry of $CeCoIn_5$ and $CeRhIn_5$ [51], it is likely that the pairing interaction in both compounds has 2D character and peaks around the same wave number on the Fermi surface. Furthermore, it has been assumed that 2D magnetic fluctuations are strong in $CeRhIn_5$. Thus, superconductivity in the $CeCoIn_5$ BLs of $CeCoIn_5(n)/CeRhIn_5(n)$ is strongly influenced. On the other hand, AFM fluctuations having 3D character in $CeIn_3$ may not play an important role for the pairing interaction in $CeCoIn_5$, resulting in little change of the superconductivity in $CeCoIn_5/CeIn_3$.

V. SUMMARY

A state-of-the-art MBE technique has enabled us to fabricate superlattices consisting of different heavy-fermion compounds. These Kondo superlattices provide a unique opportunity to study the mutual interaction between unconventional superconductivity and magnetic order through the atomic interface. In hybrid Kondo superlattice $CeCoIn_5/CeIn_3$, the superconductivity in $CeCoIn_5$ BLs and AFM order in $CeIn_3$ BLs coexist in spatially separated layers. We find that each $CeIn_3$ BL is magnetically coupled by the RKKY interaction through adjacent $CeCoIn_5$ BLs. An analysis of the upper critical field under pressure reveals that the superconductivity in $CeCoIn_5$ BLs is little influenced even in the presence of abundant AFM fluctuations in the vicinity of the AFM QCP of adjacent $CeIn_3$ BLs. Thus, although the AFM fluctuations are injected into the $CeCoIn_5$ BLs from the $CeIn_3$ BLs through the interfaces, they barely influence the force binding superconducting electron pairs. This is in sharp contrast to $CeCoIn_5/CeRhIn_5$, in which the superconductivity in the $CeCoIn_5$ BLs is strongly influenced by quantum critical AFM fluctuations in $CeRhIn_5$ BLs.

It has been widely believed that 2D AFM fluctuations are important for the pairing interaction in $CeCoIn_5$. However, direct evidence was lacking. The present results provide strong support that 2D AFM fluctuations are essentially important for the unconventional superconductivity in $CeCoIn_5$.

ACKNOWLEDGMENTS

We thank K. Ishida, H. Kontani, and Y. Yanase for fruitful discussions. This work was supported by Grants-in-Aid for Scientific Research (KAKENHI) (No. 25220710, No. 15H02014, No. 15H02106, No. 17K18753, and No. 18H05227) and Innovative Areas "Topological Material Science" (No. JP15H05852) and "3D Active-Site Science" (No. 26105004) from Japan Society for the Promotion of Science (JSPS).

[1] M. Sigrist and K. Ueda, Rev. Mod. Phys. **63**, 239 (1991).
[2] *Superconductivity Volume 1: Conventional and Unconventional Superconductors, Volume 2: Novel Superconductors*, edited by K.-H. Bennemann and J. B. Ketterson (Springer, Berlin, 2008).
[3] P. Thalmeier and G. Zwicknagl, *Unconventional Superconductivity and Magnetism in Lanthanide and Actinide Intermetallic Compounds*, Handbook of the Physics and Chemistry of Rare Earths Vol. 34 (North-Holland, Amsterdam, 2005).
[4] D. J. Scalapino, Rev. Mod. Phys. **84**, 1383 (2012).
[5] G. R. Stewart, Adv. Phys. **66**, 75 (2017).
[6] B. Keimer, S. A. Kivelson, M. R. Norman, S. Uchida, and J. Zaanen, Nature (London) **518**, 179 (2015).
[7] P. J. Hirschfeld, M. M. Korshunov, and I. I. Mazin, Rep. Prog. Phys. **74**, 124508 (2011).
[8] S. Onari and H. Kontani, *Iron-Based Superconductivity*, edited by P. D. Johnson, G. Xu, and W.-G. Yin (Springer-Verlag, Berlin, 2015).
[9] N. D. Mathur, F. M. Grosche, S. R. Julian, I. R. Walker, D. M. Freye, R. K. W. Haselwimmer, and G. G. Lonzarich, Nature (London) **394**, 39 (1998).
[10] T. Shibauchi, A. Carrington, and Y. Matsuda, Annu. Rev. Condens. Matter Phys. **5**, 113 (2014).
[11] K. Hashimoto, K. Cho, T. Shibauchi, S. Kasahara, Y. Mizukami, R. Katsumata, Y. Tsuruhara, T. Terashima, H. Ikeda, M. A. Tanatar *et al.*, Science **336**, 1554 (2012).
[12] G. Knebel, D. Aoki, J.-P. Brison, and J. Flouquet, J. Phys. Soc. Jpn. **77**, 114704 (2008).
[13] T. Park, F. Ronning, H. Q. Yuan, M. B. Salamon, R. Movshovich, J. L. Sarrao, and J. D. Thompson, Nature (London) **440**, 65 (2006).
[14] H. Shishido, T. Shibauchi, K. Yasu, T. Kato, H. Kontani, T. Terashima, and Y. Matsuda, Science **327**, 980 (2010).
[15] M. Shimozawa, S. K. Goh, T. Shibauchi, and Y. Matsuda, Rep. Prog. Phys. **79**, 074503 (2016).
[16] C. Petrovic, P. G. Pagliuso, M. F. Hundley, R. Movshovich, J. L. Sarrao, J. D. Thompson, Z. Fisk, and P. Monthoux, J. Phys.: Condens. Matter **13**, L337 (2001).
[17] Y. Mizukami, H. Shishido, T. Shibauchi, M. Shimozawa, S. Yasumoto, D. Watanabe, M. Yamashita, H. Ikeda, T. Terashima, H. Kontani, and Y. Matsuda, Nat. Phys. **7**, 849 (2011).
[18] S. K. Goh, Y. Mizukami, H. Shishido, D. Watanabe, S. Yasumoto, M. Shimozawa, M. Yamashita, T. Terashima, Y. Yanase, T. Shibauchi, A. I. Buzdin, and Y. Matsuda, Phys. Rev. Lett. **109**, 157006 (2012).
[19] M. Shimozawa, S. K. Goh, R. Endo, R. Kobayashi, T. Watashige, Y. Mizukami, H. Ikeda, H. Shishido, Y. Yanase, T. Terashima, T. Shibauchi, and Y. Matsuda, Phys. Rev. Lett. **112**, 156404 (2014).
[20] T. Ishii, R. Toda, Y. Hanaoka, Y. Tokiwa, M. Shimozawa, Y. Kasahara, R. Endo, T. Terashima, A. H. Nevidomskyy, T. Shibauchi, and Y. Matsuda, Phys. Rev. Lett. **116**, 206401 (2016).
[21] M. Naritsuka, T. Ishii, S. Miyake, Y. Tokiwa, R. Toda, M. Shimozawa, T. Terashima, T. Shibauchi, Y. Matsuda, and Y. Kasahara, Phys. Rev. B **96**, 174512 (2017).
[22] M. Naritsuka, P. F. S. Rosa, Y. Luo, Y. Kasahara, Y. Tokiwa, T. Ishii, S. Miyake, T. Terashima, T. Shibauchi, F. Ronning, J. D. Thompson, and Y. Matsuda, Phys. Rev. Lett. **120**, 187002 (2018).
[23] R. Settai, T. Takeuchi, and Y. Onuki, J. Phys. Soc. Jpn. **76**, 051003 (2007).
[24] Y. Kawasaki, S. Kawasaki, M. Yashima, T. Mito, G. Zheng, Y. Kitaoka, H. Shishido, R. Settai, Y. Haga, and Y. Onuki, J. Phys. Soc. Jpn. **72**, 2308 (2003).
[25] S. Raymond and G. Lapertot, Phys. Rev. Lett. **115**, 037001 (2015).
[26] K. Izawa, H. Yamaguchi, Y. Matsuda, H. Shishido, R. Settai, and Y. Ōnuki, Phys. Rev. Lett. **87**, 057002 (2001).
[27] K. An, T. Sakakibara, R. Settai, Y. Ōnuki, M. Hiragi, M. Ichioka, and K. Machida, Phys. Rev. Lett. **104**, 037002 (2010).
[28] Y. Matsuda, K. Izawa, and I. Vekhter, J. Phys.: Condens. Matter **18**, R705 (2006).
[29] C. Stock, C. Broholm, J. Hudis, H. J. Kang, and C. Petrovic, Phys. Rev. Lett. **100**, 087001 (2008).
[30] B. B. Zhou, S. Misra, E. H. da Silva Neto, P. Aynajian, R. E. Baumbach, J. D. Thompson, E. D. Bauer, and A. Yazdani, Nat. Phys. **9**, 474 (2013).
[31] M. P. Allan, F. Massee, D. K. Morr, J. Van Dyke, A. W. Rost, A. P. Mackenzie, C. Petrovic, and J. C. Davis, Nat. Phys. **9**, 468 (2013).
[32] T. Tayama, A. Harita, T. Sakakibara, Y. Haga, H. Shishido, R. Settai, and Y. Ōnuki, Phys. Rev. B **65**, 180504(R) (2002).
[33] A. Bianchi, R. Movshovich, N. Oeschler, P. Gegenwart, F. Steglich, J. D. Thompson, P. G. Pagliuso, and J. L. Sarrao, Phys. Rev. Lett. **89**, 137002 (2002).
[34] Y. Matsuda and H. Shimahara, J. Phys. Soc. Jpn. **76**, 051005 (2007).
[35] V. A. Sidorov, M. Nicklas, P. G. Pagliuso, J. L. Sarrao, Y. Bang, A. V. Balatsky, and J. D. Thompson, Phys. Rev. Lett. **89**, 157004 (2002).
[36] Y. Nakajima, H. Shishido, H. Nakai, T. Shibauchi, K. Behnia, K. Izawa, M. Hedo, Y. Uwatoko, T. Matsumoto, R. Settai, Y. Onuki, H. Kontani, and Y. Matsuda, J. Phys. Soc. Jpn. **76**, 024703 (2007).
[37] J. L. Sarro and J. D. Thomspson, J. Phys Soc. Jpn. **76**, 051013 (2007).
[38] T. Yamanaka, M. Shimozawa, R. Endo, Y. Mizukami, H. Shishido, T. Terashima, T. Shibauchi, Y. Matsuda, and K. Ishida, Phys. Rev. B **92**, 241105(R) (2015).
[39] D. Maruyama, M. Sigrist, and Y. Yanase, J. Phys. Soc. Jpn. **81**, 034702 (2012).
[40] G. Nakamine, T. Yamanaka, S. Kitagawa, M. Naritsuka, T. Ishii, T. Shibauchi, T. Terashima, Y. Kasahara, Y. Matsuda, and K. Ishida, Phys. Rev. B **99**, 081115(R) (2019).
[41] A. Benoit, J. X. Boucherle, P. Convert, J. Flouquet, J. Pellau, and J. Schweizer, Solid State Commun. **34**, 293 (1980).
[42] G. Knebel, D. Braithwaite, P. C. Canfield, G. Lapertot, and J. Flouquet, Phys. Rev. B **65**, 024425 (2001).
[43] T. Ebihara, I. Umehara, A. K. Albessard, K. Satoh, and Y. Onuki, Physica B **186–188**, 123 (1993).
[44] N. Harrison, U. Alver, R. G. Goodrich, I. Vekhter, J. L. Sarrao, P. G. Pagliuso, N. O. Moreno, L. Balicas, Z. Fisk, D. Hall *et al.*, Phys. Rev. Lett. **93**, 186405 (2004).
[45] N. R. Werthamer, E. Helfand, and P. C. Hohenberg, Phys. Rev. **147**, 295 (1966).

[46] E. Bauer and M. Sigrist, *Non-Centrosymmetric Superconductors: Introduction and Overview*, Lecture Notes in Physics (Springer-Verlag, Berlin, 2012).

[47] S. Fujimoto, J. Phys. Soc. Jpn. **76**, 051008 (2007).

[48] G. Knebel, M.-A. Méasson, B. Salce, D. Aoki, D. Braithwaite, J. P. Brison, and J. Flauquet, J. Phys.: Condens. Matter **16**, 8905 (2004).

[49] W. Bao, P. G. Pagliuso, J. L. Sarrao, J. D. Thompson, Z. Fisk, J. W. Lynn, and R. W. Erwin, Phys. Rev. B **62**, R14621 (2000).

[50] S. Raymond, G. Knebel, D. Aoki, and J. Flouquet, Phys. Rev. B **77**, 172502 (2008).

[51] T. Park, E. D. Bauer, and J. D. Thompson, Phys. Rev. Lett. **101**, 177002 (2008).